



Volume reduction without neuronal loss in the primate pulvinar complex following striate cortex lesions

Jonathan M. Chan^{1,2} · Katrina H. Worthy¹ · Marcello G. P. Rosa^{1,2} · David H. Reser^{2,3} · Nafiseh Atapour^{1,2}

Received: 7 March 2021 / Accepted: 13 July 2021 / Published online: 29 July 2021
© The Author(s), under exclusive licence to Springer-Verlag GmbH Germany, part of Springer Nature 2021

Abstract

Lesions in the primary visual cortex (V1) cause extensive retrograde degeneration in the lateral geniculate nucleus, but it remains unclear whether they also trigger any neuronal loss in other subcortical visual centers. The inferior (IPul) and lateral (LPul) pulvinar nuclei have been regarded as part of the pathways that convey visual information to both V1 and extrastriate cortex. Here, we apply stereological analysis techniques to NeuN-stained sections of marmoset brain, in order to investigate whether the volume of these nuclei, and the number of neurons they comprise, change following unilateral long-term V1 lesions. For comparison, the medial pulvinar nucleus (MPul), which has no connections with V1, was also studied. Compared to control animals, animals with lesions incurred either 6 weeks after birth or in adulthood showed significant LPul volume loss following long (> 11 months) survival times. However, no obvious areas of neuronal degeneration were observed. In addition, estimates of neuronal density in lesioned hemispheres were similar to those in the non-lesioned hemispheres of same animals. Our results support the view that, in marked contrast with the geniculocortical projection, the pulvinar pathway is largely spared from the most severe long-term effects of V1 lesions, whether incurred in early postnatal or adult life. This difference can be linked to the more divergent pattern of pulvinar connectivity to the visual cortex, including strong reciprocal connections with extrastriate areas. The results also caution against interpretation of volume loss in brain structures as a marker for neuronal degeneration.

Keywords Pulvinar · Volume loss · Neuronal density · Marmoset · Striate cortex lesions

Introduction

Damage to the primary visual cortex (V1) can often occur due to stroke or trauma, leading to cortical blindness (Pollock et al. 2011; Melnick et al. 2016; Hagan et al. 2017). Over subsequent months, V1 lesions also lead to significant neuronal loss due to retrograde degeneration in the lateral geniculate nucleus (LGN) and retina (Dineen and Hendrickson 1981; Cowey et al. 2011; Hendrickson et al. 2015).

This is accompanied by significant volume loss in the LGN (Atapour et al. 2017) and thinning of the retina (Meier et al. 2015). However, the possible effects of V1 lesions on other components of the visual pathway have been the subject of less study. Of particular interest is the pulvinar complex, which receives visual information both via the superior colliculus (Harting et al. 1980; Stepniewska et al. 2000; Berman and Wurtz 2010, 2011) and directly from the retina (Warner et al. 2010), and forms extensive projections to both striate and extrastriate visual areas (macaque: Ungerleider et al. 1984; Adams et al. 2000; Shipp 2001, marmoset: Dick et al. 1991; Huo et al. 2019).

The pulvinar is the largest nuclear complex of the primate thalamus, (Chalfin et al. 2007; Gutierrez et al. 2000), comprising four traditional anatomical subdivisions (inferior, lateral, medial, and anterior; Walker 1938; Jones 2007; Paxinos et al. 2012), each having different cortical connectivity (Stepniewska and Kaas 1997; Jones 2007; Baldwin et al. 2017). The medial pulvinar (MPul) nucleus has few or no connections to V1, but is connected to a wide expanse of

✉ Nafiseh Atapour
nafiseh.atapour@monash.edu

¹ Department of Physiology and Neuroscience Program, Biomedicine Discovery Institute, Monash University, Melbourne, VIC 3800, Australia

² Australian Research Council, Centre of Excellence for Integrative Brain Function, Monash University Node, Melbourne, VIC 3800, Australia

³ Graduate Entry Medicine Program, Monash Rural Health-Churchill, Churchill, VIC 3842, Australia

temporal, parietal, cingulate, and frontal cortices, including higher-order visual association areas (macaque: Trojanowski and Jacobson 1997; Gutierrez et al. 2000; marmoset: Homman-Ludiye et al. 2020). Similarly, the anterior (or oral) pulvinar has no connections with V1, being functionally connected primarily with somatic and motor processing areas (Grieve et al. 2000), including oculomotor control areas (macaque: Pons and Kaas 1985; Cusick et al. 1990; marmoset: Burman et al. 2015). In contrast, both the lateral (LPul) and the inferior pulvinar (IPul) nuclei have reciprocal connections with V1 and many extrastriate areas (macaque: Benevento and Rezak 1976; Ungerleider et al. 1983; Adams et al. 2000; Shipp 2001; marmoset: Dick et al. 1991; Huo et al. 2019; squirrel monkey: Cusick et al. 1993; Ogren and Hendrickson 1976; owl monkey: Beck and Kaas 1998; *Cebus* monkey: Soares et al. 2001). The LPul has a documented role in modulating visual responsiveness in primate V1 (Purushothaman et al. 2012), while the IPul is itself a complex formed by various subnuclei, with different neurochemical characteristics and connections to visual cortex (Baldwin et al. 2017; Mundinano et al. 2019). In macaques, both the IPul and LPul receive ascending visual input from the superior colliculus (Harting et al. 1980), which is relayed to visual cortex (Berman and Wurtz 2010, 2011).

The present study asks if V1 lesions in marmoset monkeys also trigger neuronal loss in the pulvinar complex. Evidence from some double-labeling retrograde tracer injection studies in macaque indicate that single neurons in the visual pulvinar can form synapses with multiple visual areas, including V1 (Kennedy and Bullier 1985; Lysakowski et al. 1988). This distributed organization could minimize the chances of complete removal of synaptic targets by V1 lesions, hence explaining why retrograde neuronal loss akin to that observed in the LGN has not been observed in the visual pulvinar. However, a study in marmoset monkeys has indicated that double-labeled cells in the pulvinar are observed only following injections in nearby locations in the cortex, within the likely range of the arborizations of thalamocortical axons (Kaske et al. 1991). On balance, these studies suggest that pulvinar neurons with exclusive projections to V1 could exist, a result that would lead to the expectation of some degree of retrograde degeneration within this nucleus after V1 lesion. However, the existence of these neurons, or their prevalence, has not been established.

In addition, we investigate whether there is a differential effect of V1 lesions incurred at different ages on the pulvinar. Lesions occurring in infancy reportedly cause more serious degeneration of the retina in marmosets (Hendrickson et al. 2015). The extrageniculate pathway via the pulvinar complex undergoes significant synaptic pruning as part of postnatal development (Warner et al. 2015), yielding ample opportunities for differential remodeling following V1

lesions which may enable different types of residual vision (Bourne and Morrone 2017).

Materials and methods

Animals

Eighteen marmoset monkeys (*Callithrix jacchus*) were used in this study (Table 1). Twelve animals received partial unilateral lesions of left V1, either at 6 weeks of age (neonatal lesions, $n=6$) or soon after sexual maturity (young adult lesions, $n=6$), while six non-operated, normal adults were used for comparison. The neonatal lesions were placed at the sixth week of life since it coincides with a period of rapid growth, synaptogenesis and cellular remodeling in marmoset V1 (Missler et al. 1993a, b; Bourne et al. 2005). The experiments were conducted in accordance with the Australian Code of Practice for the Care and Use of Animals for Scientific Purposes. All procedures were approved by the Monash University Animal Ethics Experimentation Committee, which also monitored the health and well-being of the animals throughout the experiments.

V1 lesions

The procedure for V1 lesions was similar to that used in previous studies (Rosa et al. 2000; Yu et al. 2013, 2018; Atapour et al. 2017), with slight refinements incorporated to the drug administration protocol. The day before surgery, animals were pre-medicated with oral meloxicam (Metacam; Boehringer Ingelheim, 0.01 mg/kg (neonates) or 0.1 mg/kg (adults) and cephalexin (Ibilex; Alphapharm P/L, 30 mg/kg). On the day of the surgery an intramuscular (i.m.) injection of atropine (Atrosite; Ilium, 0.2 mg/kg) was administered (adult animals only) 30 min prior to the induction of anesthesia with 2–5% isoflurane (Isorrane; Baxter) in oxygen. Dexamethasone (Dexason; Ilium, 0.3 mg/kg, i.m.) was also administered before the animals were positioned in a modified stereotaxic head holder. Body temperature, heart rate, and blood oxygenation (PO_2) were continually monitored, and the rate of anesthetic was continuously adjusted (isoflurane 2–5%) to maintain areflexia, relaxed breathing, and low heart rates. Under sterile conditions, a craniotomy was made over the occipital pole of the left hemisphere. Using a fine-tipped cautery, an excision was then made of all cortical tissue caudal to a plane extending from the dorsal surface of the occipital lobe to the cerebellar tentorium, across its entire mediolateral extent (Rosa et al. 2000; see Fig. 1). This type of lesion removes the central visual field representation in the occipital operculum, as well as of the peripheral representation (in the calcarine sulcus) up to a

Table 1 Animal details

| Group | Case | Sex | Body weight (g) | Age at lesion (weeks) | Survival time post lesion (months) | Age at perfusion (months) |
|-------------------|------------------|-----|-----------------|-----------------------|------------------------------------|---------------------------|
| Control | CJ167 | F | 390.0 | – | – | 27 |
| | CJ173 | M | 340.0 | – | – | 24 |
| | CJ198 | M | 383.0 | – | – | 32 |
| | CJ200 | F | 441.0 | – | – | 43 |
| | CJ204 | M | 426.0 | – | – | 41 |
| | CJ1741 | F | 309.0 | – | – | 40 |
| Neonate -lesioned | W6G | M | 376.0 | 6 | 24 | 25 |
| | W6H | F | 301.0 | 6 | 20 | 21 |
| | W6I | M | 447.0 | 6 | 28 | 29 |
| | W6K ^a | M | 389.0 | 6 | 31 | 33 |
| | W6L | F | 375.0 | 6 | 33 | 35 |
| | W6M | M | 354.0 | 6 | 32 | 34 |
| Adult-lesioned | WA6 | M | 388.0 | 107 | 17 | 41 |
| | WA8 | M | 358.0 | 82 | 14 | 33 |
| | WA13 | M | 366.0 | 122 | 28 | 56 |
| | WA14 | F | 410.0 | 110 | 30 | 55 |
| | WA15 | F | 346.0 | 113 | 11 | 37 |
| | WA16 | M | 434.0 | 137 | 22 | 54 |

^aUsed for volume analysis only

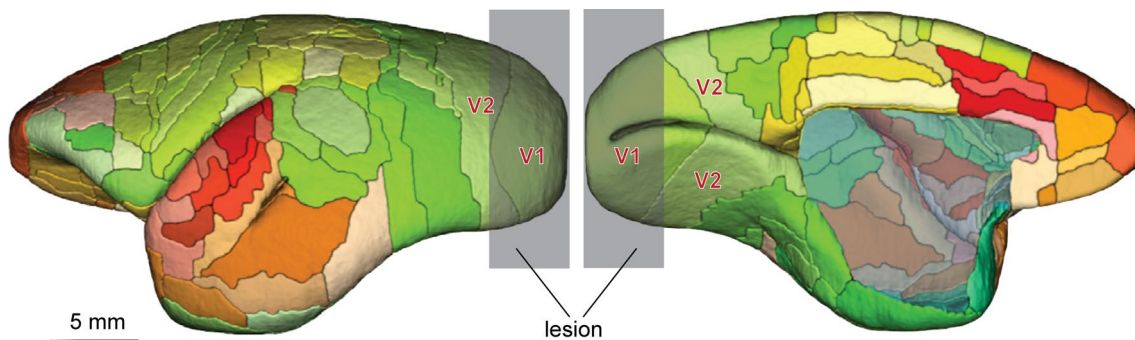


Fig. 1 Extent of the intended lesions, depicted in lateral (left) and medial (right) views of the marmoset cortex. The diagrams are based on an average template of the marmoset brain (Majka et al. 2021), with colors indicating different cortical areas. The locations of the primary (V1) and second (V2) visual areas are indicated. The lesions (gray shading) were intended to remove the entire representation of the central visual field in V1, in the occipital operculum, as well as

the caudal part of the calcarine sulcus. Based on electrophysiological recordings in other animals with similar lesions (Yu et al. 2013, 2018), this creates a contralateral scotoma that extends at least to 40° eccentricity along the horizontal meridian of the visual field. The lesions also involved V2 to variable extents. For histological documentation of lesion extents, see Atapour et al. (2021)

minimum of 40° eccentricity along the horizontal meridian (Chaplin et al. 2013; Atapour et al. 2021). This corresponds to a minimum of 70% of V1, while sparing the majority of secondary visual area (V2) except for the border region with V1 in the central representation (as determined by electrophysiology; Yu et al. 2018). After application of hemostatic microspheres (Arista AH; BARD Davol Inc), the surfaces of the exposed occipital cortex and tentorium were protected with ophthalmic film (Gelfilm; Pfizer Inc), and the

cavity was filled with Gelfoam (Pfizer Inc). The skull flap was repositioned and secured with cyanoacrylate (Vetbond; 3M), and the skin was sutured. The marmosets were placed in a humidicrib until recovery of movement, after which they were returned to the mothers (neonatal animals) and, in all cases, subsequently reintroduced to the colony. Post-operative analgesic (oral meloxicam 0.005 mg/kg neonates, 0.05 mg/kg adults, 3 days) and antibiotic (oral cephalixin 30 mg/kg, 5 days) were administered.

Throughout the post-lesion period, the marmosets were housed in large cages with family groups, having access to both indoor and outdoor environments. During the survival period all animals demonstrated normal patterns of movement, including the capacity to perform fine grasping and holding movements and to perform precise jumps across tree branches, and did not require assistance for daily activities such as seeking and obtaining food.

Tissue processing

Following survival times of 11–33 months (and in some cases, tracer injections not related to the present study), the animals were anesthetized with alfaxalone (10 mg/ml i.m.), and administered an overdose of sodium pentobarbitone (100 mg/kg, i.v.) after the loss of consciousness. They were then immediately perfused through the heart with heparinised saline, followed by 4% paraformaldehyde (PFA) in 0.1 M phosphate-buffered saline (PBS; pH 7.4). The brains were post-fixed in the same medium for at least 24 h and then immersed in buffered paraformaldehyde with increasing sucrose concentrations (10–30%). They were then sectioned (40 μm thickness) in the coronal plane using a cryostat. Adjacent sections were stained for Nissl substance, NeuN (Wolf et al. 1996), and myelin (Gallyas 1979) following standard protocols (Fig. 2A). The spacing between adjacent sections in each series was 200 μm . For NeuN staining, the sections were incubated in blocking solution (10% normal horse serum and 0.3% Triton X-100 in 0.1 M PBS) for 1 h at room temperature and then incubated with the primary antibody for NeuN (1:800, MAB377, Merck Millipore) at 4 °C for 42–46 h. Secondary antibody (1:200, PK-6102, Vectastain Elite ABC HRP kit, Vector Laboratories) was applied for 30 min at room temperature followed by avidin/biotin interaction and DAB (DAB Peroxidase Substrate Kit SK-4100, Vector Laboratories) staining. The remaining sections in each series were stored in cryoprotectant solution as a backup for unsatisfactory staining or damaged histological sections, or used for other stains (not reported here).

Identification of the medial, lateral and inferior pulvinar nuclei

Utilizing NeuN and myelin staining, we delineated the IPul, LPul and MPul using the Paxinos et al. (2012) atlas as the main guide. The characteristics of the pulvinar nuclei in the marmoset were consistent with previous descriptions in the macaque (Adams et al. 2000; Gutierrez et al. 2000; Jones 2007). The MPul is lightly myelinated (Fig. 2A, right), and has a relatively homogeneous cytoarchitecture composed of small- to medium-sized neurons which stain homogeneously for NeuN (Fig. 2A, left and Fig. 2B). These features helped differentiate MPul from the neighboring structures. The

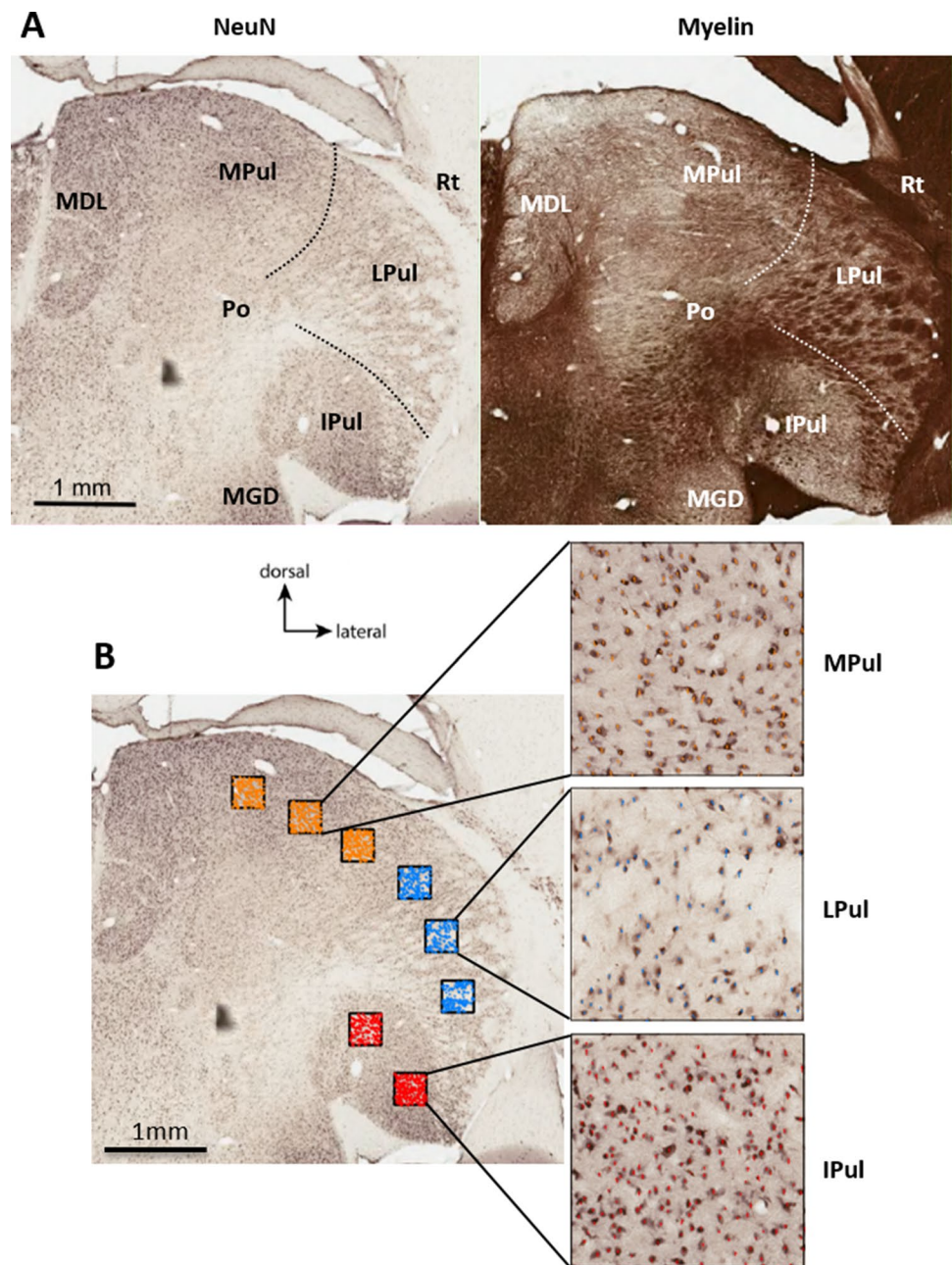
LPul has a distinctive pattern of myelinated fiber bundles running across its extent (Fig. 2A), resulting in variations in neuronal density, and shows a more diverse range of neuron sizes and cell body shapes in the NeuN stain (Fig. 2B). We defined the IPul according to the modern consensus (Stepniewska and Kaas 1997; Adams et al. 2000; Gutierrez et al. 2000; Soares et al. 2001; Mundinano et al. 2019) whereby this nucleus has heterogeneous myelination, including some densely myelinated patches (Fig. 2A), reflecting a proposed parcellation into subnuclei (Baldwin et al. 2017). In NeuN-stained sections (Fig. 2A, left and Fig. 2B), IPul neurons appear as darkly stained, are tightly packed, and encompass a larger range of cell body sizes in comparison with the LPul. For the purposes of the present analysis the IPul was assessed as a single structure. Figure 3 (left) illustrates the extent of the three subdivisions included in this study in a series of coronal sections from a non-lesioned animal (case CJ1741).

Volume and neuron density measurement

Sections containing the pulvinar were scanned using an Aperio Scanscope AT Turbo at 20 \times magnification. The outlines of the IPul, LPul and MPul were drawn on NeuN-stained sections using the Aperio ImageScope software (Aperio Technologies V12.1.0.5029) (Figs. 2, 3). An estimate of the pulvinar volume was obtained using the Cavalieri estimator method (Gundersen and Jensen 1987; Royet 1991), based on equally spaced sections through the nucleus. The pulvinar's total volume was calculated based on the sum of volumes obtained for each section (pulvinar area \times distance between sections). Measurements were corrected with a shrinkage factor of 0.8 (Atapour et al. 2017).

Sampling for neuronal counts was performed using previously described methods (Williams and Rakic 1988; Atapour et al. 2017, 2019). All available sections including the full anteroposterior extent of the IPul, LPul and MPul were sampled. Counting frames (300 \times 300 μm^2) were evenly spaced along the radial dimension of the pulvinar (Fig. 2B). Given the currently acknowledged structural and functional similarity between the LPul and the most lateral part of the IPul (subnucleus P1c1 in Kaas and Baldwin 2020), we avoided including the latter. In addition, the fringes of the nuclear masses were avoided, to prevent sampling that could include regions outside the boundaries. Neurons were identified within each frame based on two exclusion lines (right and top), and two inclusion lines (bottom and left). Neurons were counted if they were entirely within the counting frames or crossed the inclusion lines. Only neurons with evident nuclear staining, independent of size and shape, were counted. Numbers of neurons in each counting frame were divided by volume to calculate neuronal density. Neuronal density from each section along the anterior–posterior extent

Fig. 2 **A** Example coronal sections stained for the neuronal marker NeuN (left) and for myelin (right) corresponding to the interaural level +3.00 mm in the Paxinos atlas (Paxinos et al. 2012), in which the medial (MPul), lateral (LPul) and inferior pulvinar (IPul) subdivisions are indicated. MDL (Mediodorsal thalamic nucleus, lateral part), MGD (Medial geniculate nucleus, dorsal part), Po (Posterior thalamic nuclear group), Rt (Reticular nucleus). **B** The location of sampling grids (300 × 300 μm²) on a representative NeuN-stained coronal section. Insets show magnified examples of neurons counted in each counting grid for the three subdivisions



of the pulvinar was compared among control, neonate and adult V1 lesion cases, to determine if natural variations (or differential effects of degeneration) occurred in a specific region along this axis. The volumes of the LGN were also measured to facilitate comparison with past studies.

Statistical analyses

For statistical analysis of the volume of pulvinar subdivisions, neuronal density and neuron number, we used one-way ANOVAs followed by post hoc Tukey's tests. A repeated-measure two-way ANOVA was used to assess

interhemispheric differences of neuronal density in the pulvinar nuclei ipsi- and contralateral to the lesions. Simple linear regression was used for analysis shown in Figs. 5 and 8. Data are presented as mean ± SD and differences with $p < 0.05$ were considered statistically significant.

Results

The present study is based on comparisons between the IPul, LPul and MPul nuclei of non-lesioned (control) marmosets and both hemispheres of those that had unilateral V1 lesions

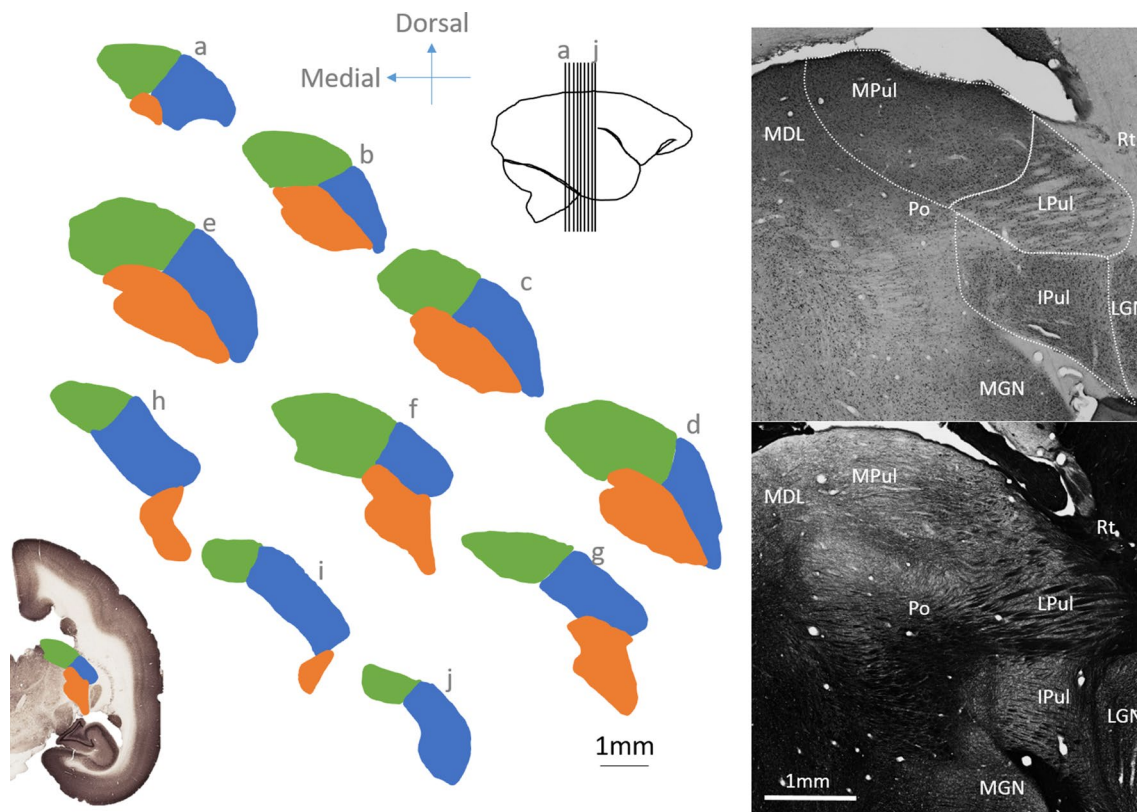


Fig. 3 Delineation of marmoset pulvinar. Left: Diagrammatic representation of the three subdivisions of the marmoset pulvinar [medial (MPul)—green, lateral (LPul)—blue, inferior (IPul)—orange] from posterior to the anterior (a–j), in coronal sections. Each section is approximately 200 μm apart. Bottom left section displays a representative coronal section stained for NeuN (neuronal marker) where the locations of the pulvinar nuclei are indicated. Top right inset shows

the coronal levels at which the sections were obtained. Right: NeuN (top) and myelin (bottom) stained coronal sections showing borders of MPul, LPul, and IPul relative to adjacent nuclei. MDL (Mediodorsal thalamic nucleus, lateral part), MG (Medial geniculate nucleus), Po (Posterior thalamic nuclear group), Rt (Reticular nucleus), LGN (Lateral geniculate nucleus)

either at 6 weeks of age or young adulthood. Because the MPul does not have connections with either V1 or caudal extrastriate areas, this nucleus was included in the analyses for comparison, to assess the hypothesis that any changes that resulted specifically from the V1 lesions would affect only the IPul and LPul.

Pulvinar volume

In control (non-lesioned) animals, the combined volume of the MPul, LPul and IPul was $22.3 \pm 1.8 \text{ mm}^3$ (mean \pm SD, Fig. 4A). This value was comparable to that of a previous report in which delineations were also based on the Paxinos et al. (2012) marmoset atlas (Warner et al. 2015). In addition, the use of unilateral V1 lesions in this study allowed for the volume of the pulvinar in the hemisphere contralateral to the lesion to be used for comparisons which took into account individual variability.

Comparison of the combined volume of IPul, LPul and MPul revealed a significant reduction in the hemisphere

ipsilateral to the lesion in both neonate- and adult-lesioned animals, compared to control animals [one-way ANOVA; $F(4, 25) = 6.58$, $p = 0.0009$, Fig. 4A]. Post hoc analysis indicated the mean combined volume in the neonate- and adult-lesioned animals was significantly lower than that in control animals (mean \pm SD, Neonate-lesioned vs. Control; 17.9 ± 1.3 vs $22.3 \pm 1.8 \text{ mm}^3$, $p = 0.0009$, Adult-lesioned vs Control; 19.3 ± 2.3 vs $22.3 \pm 1.8 \text{ mm}^3$, $p = 0.03$). For the neonate-lesioned animals the whole pulvinar volume was also significantly different between the ipsi- and contralateral sides (mean \pm SD, Neonate-lesioned, Ipsilateral vs. Contralateral; 17.9 ± 1.3 vs $20.9 \pm 0.8 \text{ mm}^3$, $p = 0.02$).

Further analysis of volume loss according to subdivisions of the pulvinar (Fig. 4B–D) showed that the volume loss was largely attributable to changes in LPul, but not in the MPul and IPul. This finding was reflected in both neonate- and adult-lesioned cases [one-way ANOVA, MPul; $F(4, 25) = 0.74$, $p = 0.57$, Fig. 4B, LPul; $F(4, 25) = 10.35$, $p < 0.0001$, Fig. 4C and IPul; $F(4, 25) = 2.31$, $p = 0.08$, Fig. 4D]. Post hoc analysis indicated that mean score for

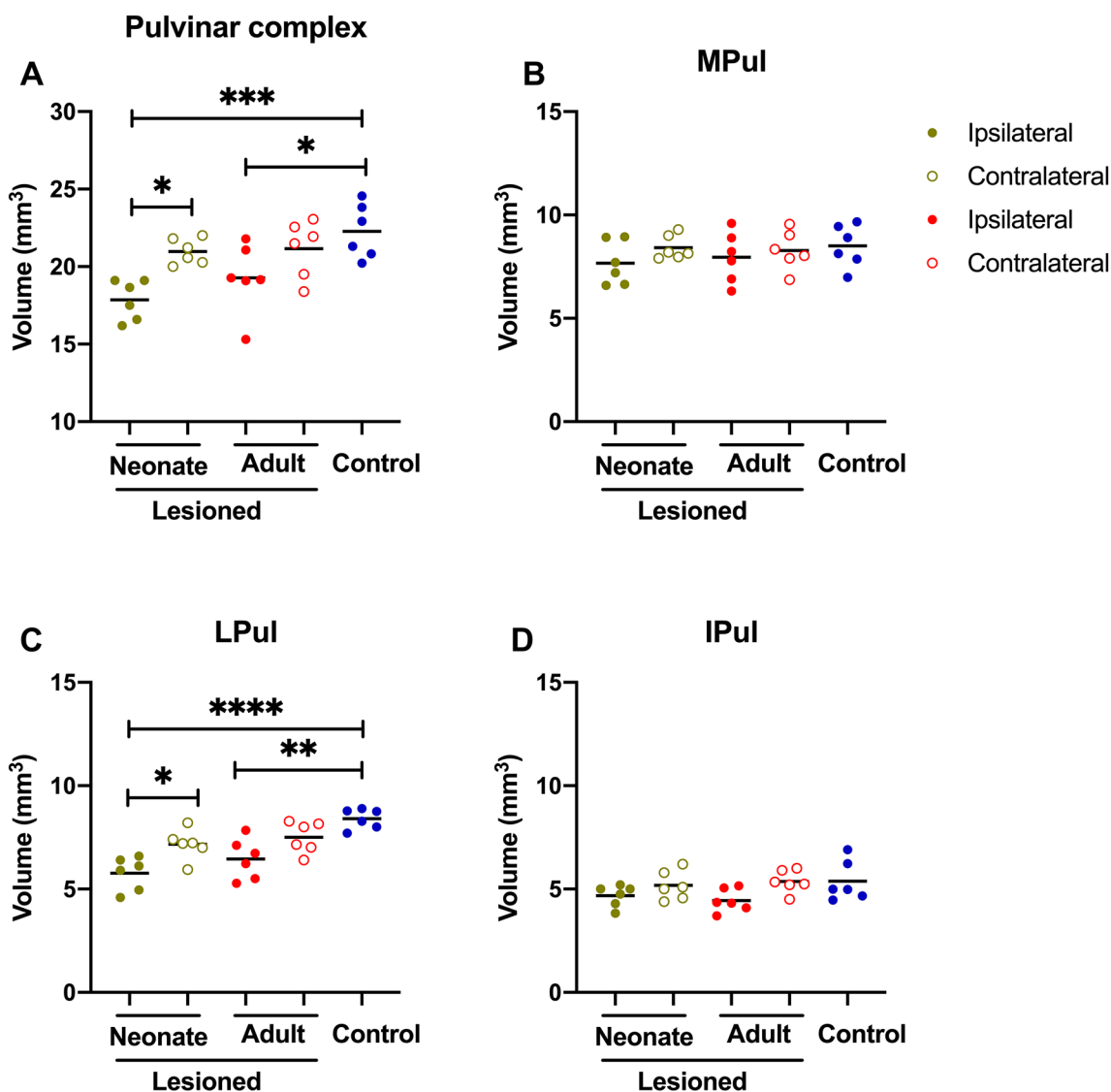


Fig. 4 Pulvinar volume in lesioned and control hemispheres. **A** Significant volume loss for the combined volume of pulvinar complex in the ipsilateral hemisphere of the neonate- and adult-lesioned animals. **B–D** Examination of pulvinar volume for the MPul, LPul and

IPul. A significant volume decrease was detected only in the LPul, of both neonate- and adult-lesioned animals. * $p < 0.05$, ** $p < 0.01$, *** $p < 0.001$, **** $p < 0.0001$. Bar indicates mean volume

LPul volume in the neonate- and adult-lesioned animals was significantly lower than that of control animals (mean \pm SD, neonate-lesioned vs control, 5.8 ± 0.8 vs 8.4 ± 0.5 mm³, $p < 0.0001$, adult-lesioned vs control; 6.5 ± 1.0 vs 8.4 ± 0.5 mm³, $p = 0.0015$). For the neonate-lesioned animals the LPul volume was also significantly different between the sides ipsi- and contralateral to the lesions (mean \pm SD, Neonate-lesioned, Ipsilateral vs. Contralateral; 5.8 ± 0.8 vs 7.2 ± 0.7 mm³, $p = 0.03$).

Volume reduction in the LGN has been reported to be proportionate to the size of V1 lesion, which makes it a useful indicator of the degree of V1 loss (Hendrickson et al. 2015; Atapour et al. 2017). We compared estimates of the

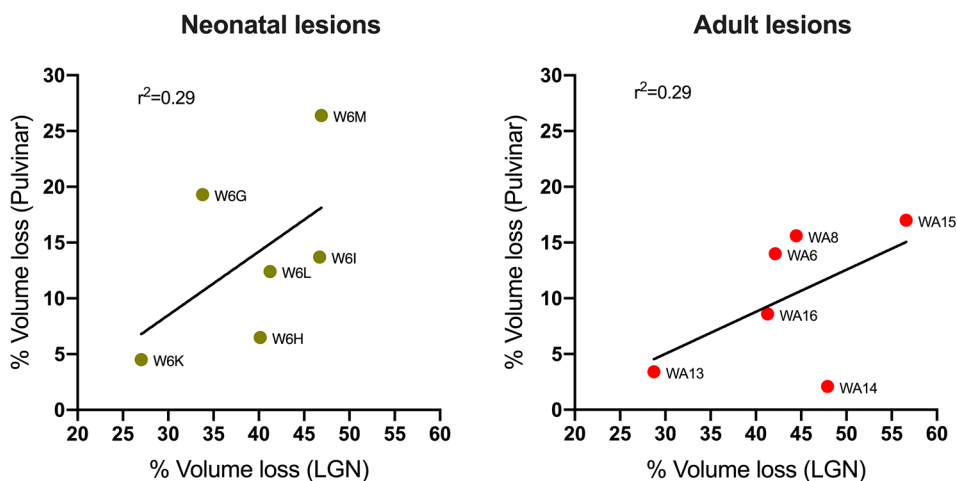
LGN volume loss with corresponding estimates of pulvinar volume loss. This analysis revealed no significant correlation (Neonate lesions; $r^2 = 0.29$, $p = 0.26$), Adult lesions ($r^2 = 0.29$, $p = 0.26$), Fig. 5).

Neuronal density

The mean neuronal density in the MPul, LPul and IPul of control animals (mean \pm SD) was 29,540 cells/mm³ (± 9437), 20,560 cells/mm³ (± 5411) and 26,860 cells/mm³ (± 7536), respectively.

To examine the effect of V1 lesions on neuronal density we calculated the averages of neuronal density from each

Fig. 5 The interhemispheric volume reduction of the pulvinar complex does not correlate with the reduction of the lateral geniculate nucleus (LGN) of the same animals. Data for both neonate- ($r^2=0.29$, $p=0.26$) and adult- ($r^2=0.29$, $p=0.26$) lesioned animals are shown separately



animal, by subdivision of the pulvinar complex, and for each hemisphere (Fig. 6). Comparison of neuronal density did not reveal any significant differences [One-way ANOVA; Pulvinar complex; $F(4, 23)=0.83$, $p=0.51$, Fig. 6A, MPul; $F(4, 23)=0.46$, $p=0.76$, Fig. 6B, LPul; $F(4, 23)=1.24$, $p=0.31$, Fig. 6C, and IPul; $F(4, 23)=1.15$, $p=0.35$, Fig. 6D)]. The results reveal that pulvinar neuronal density was not significantly affected by V1 lesions induced either at the neonatal period or adulthood.

To further investigate the effects of V1 lesions on pulvinar neuronal density, we also compared the ipsilateral and contralateral pulvinars in lesioned animals, using two-way repeated measures ANOVA. We found that despite the high variability of neuronal density among cases, the differences between the ipsilateral and contralateral pulvinar neuronal density were not significant, both in the neonatal or adult-lesioned groups [Pulvinar complex; Lesion onset age; $F(1, 5)=1.59$, $p=0.26$, Hemisphere; $F(1, 5)=4.05$, $p=0.1$, Lesion onset age \times Hemisphere; $F(1, 3)=0.28$, $p=0.62$, Fig. 7A, MPul; Lesion onset age; $F(1, 5)=1.14$, $p=0.33$, Hemisphere; $F(1, 5)=0.31$, $p=0.59$, Lesion onset age \times Hemisphere; $F(1, 3)=0.03$, $p=0.85$, Fig. 7B, LPul; Lesion onset age; $F(1, 5)=1.96$, $p=0.22$, Hemisphere; $F(1, 5)=0.01$, $p=0.90$, Lesion onset age \times Hemisphere; $F(1, 3)=0.07$, $p=0.80$, Fig. 7C) and IPul; Lesion onset age; $F(1, 5)=2.21$, $p=0.19$, Hemisphere; $F(1, 5)=1.85$, $p=0.23$, Lesion onset age \times Hemisphere; $F(1, 3)=1.19$, $p=0.35$, Fig. 7D].

Simple regression analysis showed no gradient of neuronal density across the anterior–posterior extent of the pulvinar subdivisions in control [r^2 : MPul 0.009, LPul 0.10 and IPul 0.05], neonatal lesion [r^2 : MPul 0.01, LPul 0.03 and IPul 0.04] or adult-lesioned animals [r^2 : MPul 0.05, LPul 0.15 and IPul 0.12, Fig. 8]. Slopes were not significantly different across the anterior–posterior extent of the pulvinar complex between control, neonate- and adult-lesioned animals [MPul; $F(2, 248)=2.27$, $p=0.10$, LPul;

$F(2, 249)=0.34$, $p=0.71$, IPul; $F(2, 226)=0.24$, $p=0.78$, Fig. 8]. Only data from the side ipsilateral to the lesion have been analyzed and shown in Fig. 8.

Total neuron numbers in the pulvinar

Finally, to evaluate if V1 lesions cause a loss of neurons in the pulvinar complex, estimates of the total neuron number within each section were calculated by multiplying the neuronal density in each subdivision by its volume. Although the estimates tended to be lower on average in the hemispheres ipsilateral to the lesions, this analysis did not find any significant differences in total neuron numbers across the whole pulvinar, when comparing neonate-lesioned, adult-lesioned and control animals [one-way ANOVA; $F(4, 23)=1.47$, $p=0.24$] (Fig. 9).

Discussion

We found no evidence of obvious retrograde neuronal degeneration in the pulvinar complex following V1 lesions. This finding supports the notion that cells in this complex remain capable of transferring signals to the extrastriate cortex for enabling the residual visual abilities that continue in the absence of V1 (Hagan et al. 2019). Our findings are compatible with the view that the more distributed pattern of pulvino-cortical connectivity, when compared with the geniculocortical projection, spares neurons in this complex from retrograde degeneration triggered by the full loss of synaptic targets. Further, our data on neuronal density of MPul, LPul and IPul in control marmoset monkeys provide accurate, stereology-based estimates which may be useful in models aimed at further understanding this component of the visual thalamic circuitry.

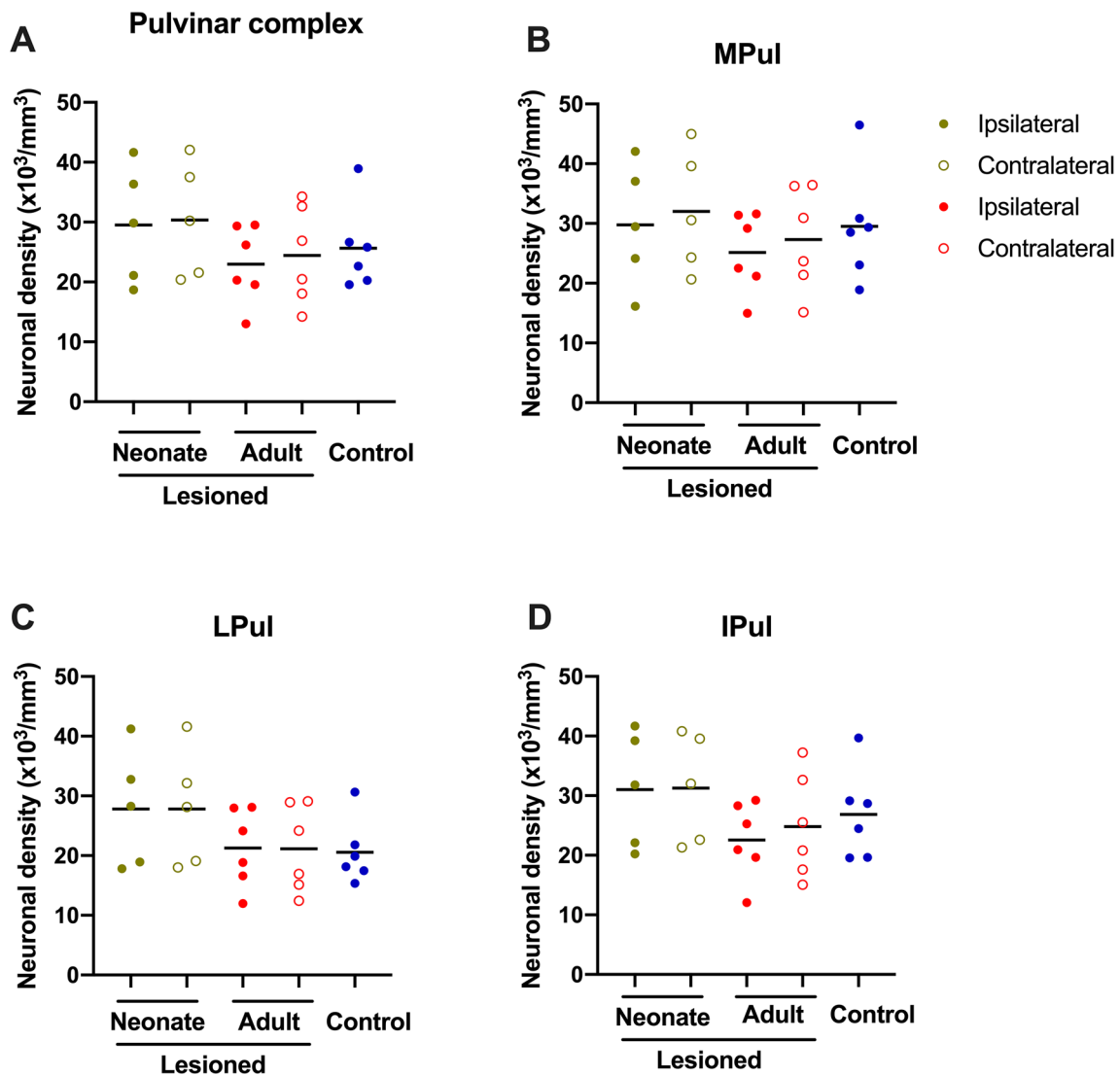


Fig. 6 Neuronal density in the pulvinar complex (A) or each subdivision investigated in the present study (B–D). No significant difference was detected between groups. Each point represents the averaged pulvinar neuronal density across all pulvinar sections of a single animal

Pulvinar volume

Our estimates of the volumes of IPul, LPul and MPul were comparable to those obtained by Warner et al. (2015). Both the IPul and LPul form projections to V1 (Adams et al. 2000; Soares et al. 2001), and therefore could be expected to be affected by lesions in this area. Yet, the small degree of volume loss in the lesioned animals was limited to the LPul. In the absence of significant cellular loss, we regard this volume reduction as most likely being due to the loss of myelinated axons, which has been observed following other types of injury and in neurodegenerative diseases (Minagar et al. 2013; Marion et al. 2019; Chen et al. 2020). The LPul is characterized by distinctive myelin-rich patches between the clusters

of neurons, and the observed shrinkage could represent the loss of axons traversing this nucleus on the way to visual structures such as the superior colliculus. Consistent with this idea, an imaging study of a macaque brain born with bilateral V1 lesions reported volume loss from the white matter tracts surrounding the pulvinar (Bridge et al. 2019). Another possible contributor to the volume loss in the LPul could be changes in the dendritic neuropil of pulvinar neurons, similar to that observed in other structures following traumatic brain injury (Ratliff et al. 2020). Although loss of cortical inputs may cause changes in the thalamic neuronal architecture, the fact that the volume loss was confined to the LPul (where the most abundant myelin tracts are found) renders this explanation less likely. Nonetheless, the fact that the LPul has an

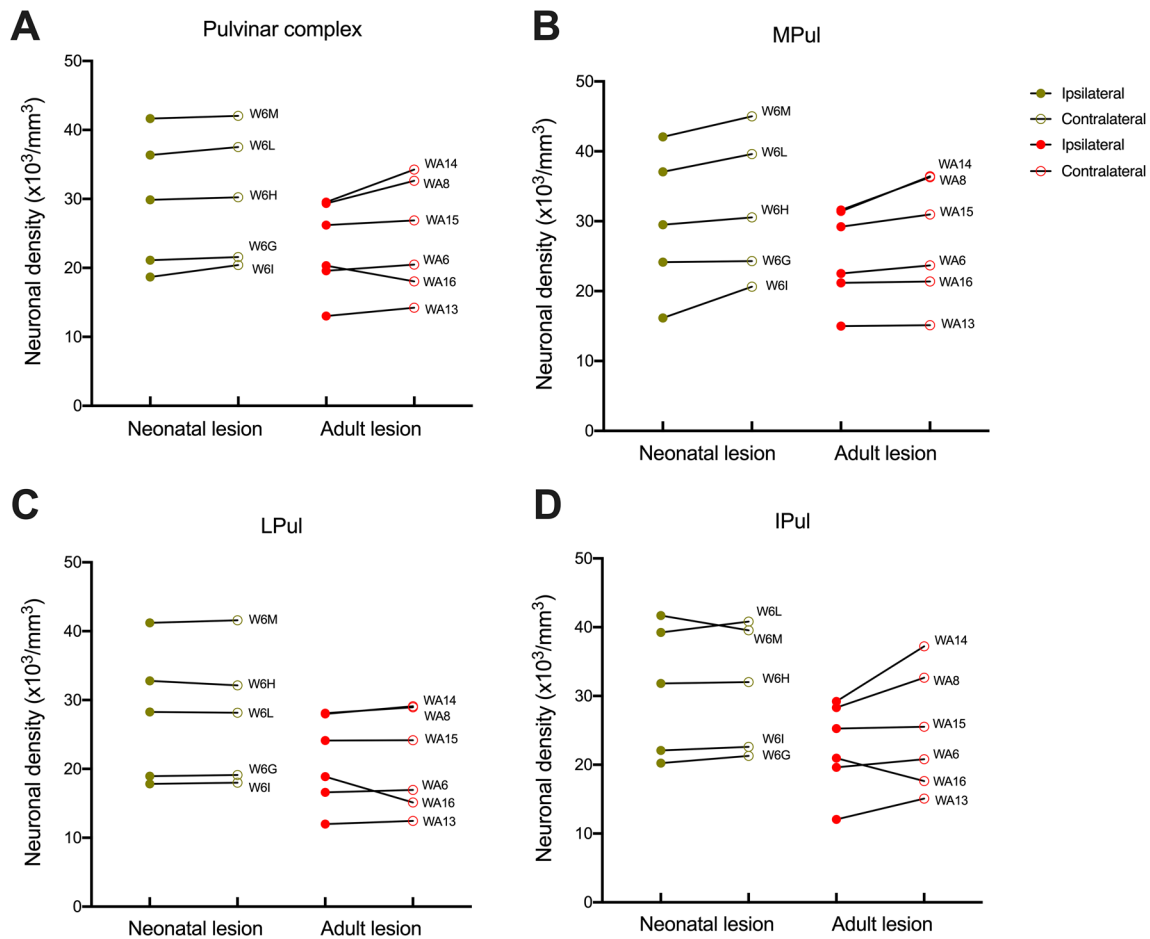


Fig. 7 Interhemispheric differences of neuronal density in the pulvinar complex (**A**) and each of its subdivisions in lesioned animals (**B–D**). Each point represents the averaged pulvinar neuronal density

across all pulvinar sections of a single animal. Note this is an interhemispheric plot of data obtained from lesioned animals shown in Fig. 6

established function in shaping neuronal responses in V1 (Purushothaman et al. 2012) indicates that this deserves further study, including neuronal filling by intracellular injection, Golgi stains, or electron microscopy techniques.

Since volume reduction in the LPul subsequent to V1 lesions does not correspond with a measurable degree of neuronal loss in the LPul, caution is required when interpreting data from neuropathological studies where volume of a neuronal structure is the only measure available. Volume measurement has been regarded as a useful tool in the assessment of severity of many brain disorders including schizophrenia (Byne et al. 2007; Kemether et al. 2003), multiple sclerosis (Mahajan et al. 2020; Pareto et al. 2020), stroke (Krishnamurthy et al. 2020), migraines (Magon et al. 2015; Shin et al. 2019), and panic disorder (Asami et al. 2018). However, our data demonstrate that this type of measurement should not be used as an indication of a proportional neuronal loss.

Pulvinar neuronal density

The present study was based on long (11–33 months) survival times following V1 lesions. Our previous studies in the LGN showed that retrograde degeneration stabilizes after a few months (Atapour et al. 2017). Thus, it is unlikely that the lack of evidence of neuronal loss in the pulvinar complex is due to insufficient time for neuronal loss to become evident.

The pulvinar nuclei have complex shapes, and the neurons therein form several retinotopic maps (Dick et al. 1991; Adams et al. 2000; Soares et al. 2001; Mundinano et al. 2019). We explored the possibility that neuronal loss would be confined to a specific region by sampling neuronal density across sections encompassing the entire anterior–posterior extent of the IPul, MPul and LPul. Although our results did not uncover evidence of localized cellular loss, they cannot exclude the possibility of localized loss confined to small regions, beyond the detection power of

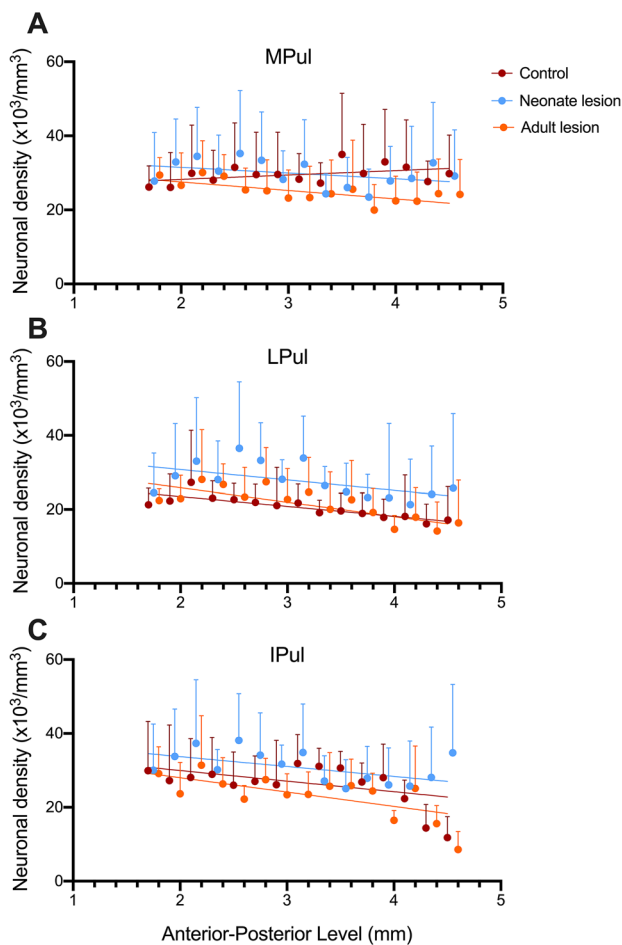


Fig. 8 Neuronal density across the anterior–posterior axis of pulvinar subdivisions. The averaged neuronal density along the posterior–anterior extent of medial pulvinar (MPul, **A**), lateral pulvinar (LPul, **B**) and inferior pulvinar (IPul, **C**) is shown for control, neonate- and adult-lesioned marmosets. Each data point is averaged neuronal density obtained from a section. Each section is 200 μm apart

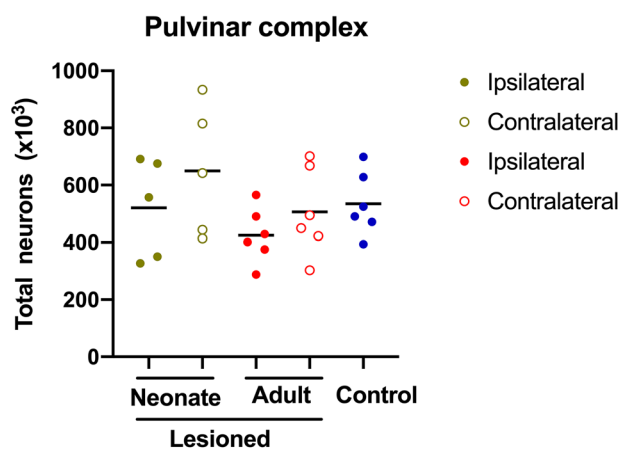


Fig. 9 Estimated number of neurons in the pulvinar complex for lesioned and control animals. Each point represents the averaged number obtained from a single animal. No significant difference was observed among groups. Bars indicates means

our sampling and analysis. In this regard, the small volume of the neurochemically distinct subdivisions of IPul (Cusick et al. 1993; Gutierrez et al 2000; Soares et al. 2001; Paxinos et al. 2012) creates challenges to the application of unbiased stereological analyses.

It is important to note that neuronal density estimates in the individuals sampled in this study were found to be variable, a fact that may partially be due to differences observed in NeuN staining. This result is somewhat puzzling, in view of the fact that estimates obtained in the LGN with similar techniques, sometimes in the same individuals, were not correspondingly variable (Atapour et al. 2017). However, despite inter-individual differences, the interhemispheric estimates of neuronal density were small in all lesioned animals, confirming that V1 lesion did not cause detectable neuronal loss. Another methodological consideration is that although our sampling frames were designed larger (> 2 times) than those used in our previous studies (Atapour et al. 2017, 2019), to account for the presence of fiber tracts. The sampled regions excluded the largest fiber tracts within the LPul, where the shrinkage may have mainly occurred. This may have contributed to the lack of changes in neuronal density (and neuronal number) in lesioned cases, despite volume loss.

Retrograde degeneration of thalamocortical neurons can mainly be attributed to the impaired retrograde axonal transport and loss of synaptic targets after axotomy (Perlson et al. 2010; Hill et al. 2016). While numerous molecular pathways and pathological processes are involved in the axonal degeneration and neuronal death (Hill et al. 2016), defective axonal transport and changes in retrograde signaling pathways are the major contributing factors (Perlson et al. 2010). Moreover, loss of corticothalamic inputs after V1 lesion may amplify neurodegeneration due to the associated reduction in synaptic activity that may influence overall neuronal function (Gao et al. 2011). In this light, the lack of degeneration in the pulvinar nuclei following V1 lesions could be explained by two main contributing factors. First, the anatomical connections of the pulvinar nuclei with V1 (in several primate species including marmoset) have been described as being less prominent, in comparison with those to extrastriate areas (Adams et al. 2000; Kaas and Lyon 2007). For example, projecting neurons in the LPul and IPul form relatively denser connections with V2 than with V1 (macaque; Benevento and Rezak 1976). In contrast, the LGN is primarily connected to V1, but has sparser connections with V2 (macaque; Bullier and Kennedy 1983) and other areas (marmoset; Huo et al. 2019). Second, there is evidence from double-labeling experiments in macaques that single pulvinar neurons may form projections to more than one area, such as V1 and V2 (Kennedy and Bullier 1985) or V1 and V4 (Lysakowski et al. 1988). These projections terminate superficially in V1, and thus are likely

of calbindin-positive, 'matrix' relay cell origin, known to terminate diffusely (Jones 2001). In addition, single-label experiments have revealed that the pulvinar projecting zones to V1 and extrastriate areas overlap extensively, reiterating a distributed connectivity (*Cebus* monkey; Soares et al. 2001). These alternative targets for pulvinar neurons could help sustain pulvinar neurons after V1 lesions, preventing retrograde degeneration. Whereas the existence or distribution of pulvinar neurons that only project to V1 has not been established, the current findings suggest that, if they exist, they must not be concentrated in a manner that leads to a circumscribed degeneration zone in this nuclear complex.

Lesions in infancy and adulthood

Our results showed no evidence of a differential effect of V1 lesions sustained in early postnatal life (6 weeks of age), versus adulthood. This is significant in view of the fact that the first of these periods is associated with developmental changes in the visual cortex (Missler et al. 1993a, b; Bourne et al. 2005; Bourne and Rosa 2006), which creates opportunity for significant rearrangement of the thalamocortical projection pattern (Warner et al. 2015). This rearrangement has been associated with better preservation of visual function following V1 lesions in infancy, compared to adulthood (Fox et al. 2020). Our results indicate that the plasticity mechanisms underlying such changes do not involve differential survival of neurons in the pulvinar.

Conclusions

In summary, our results show that the pulvinar nuclei remain relatively largely unaffected following V1 lesions either in infancy or adulthood. These findings are in line with the hypothesis that the pulvinar complex has a role in supporting residual visual capabilities (Rodman et al. 1990; Bridge et al. 2016; Takakuwa et al. 2021), but do not provide additional evidence which can be correlated to the better functional outcomes of lesions in early life. Finally, they also demonstrate that a moderate degree of volume loss can occur in a neural structure without concomitant neuronal death, a conclusion which may have practical significance in the interpretation of neuropathological mechanisms from non-invasive imaging data.

Acknowledgements The authors acknowledge the support of the Monash Histology platform, which provided slide scanning services.

Funding This research was supported by an Australian Government Research Training Program (RTP) Scholarship to JMC, and by grants from the National Health and Medical Research Council (1122220 and 1194206) to MGPR.

Declarations

Conflict of interest The authors have no conflicts of interest to declare.

Ethics approval The experiments were conducted in accordance with the Australian Code of Practice for the Care and Use of Animals for Scientific Purposes. All procedures were approved by the Monash University Animal Ethics Experimentation Committee, which also monitored the health and well-being of the animals throughout the experiments.

Consent to participate Written informed consent was obtained from all authors included in the study.

References

- Adams MM, Hof PR, Gattass R, Webster MJ, Ungerleider LG (2000) Visual cortical projections and chemoarchitecture of macaque monkey pulvinar. *J Comp Neurol* 419:377–393
- Asami T, Yoshida H, Takaishi M, Nakamura R, Yoshimi A, Whitford TJ, Hirayasu Y (2018) Thalamic shape and volume abnormalities in female patients with panic disorder. *PLoS One* 13:e0208152
- Atapour N, Worthy KH, Lui LL, Yu HH, Rosa MGP (2017) Neuronal degeneration in the dorsal lateral geniculate nucleus following lesions of primary visual cortex: comparison of young adult and geriatric marmoset monkeys. *Brain Struct Funct* 222:3283–3293
- Atapour N, Majka P, Wolkowicz IH, Malamanova D, Worthy KH, Rosa MGP (2019) Neuronal distribution across the cerebral cortex of the marmoset monkey (*Callithrix jacchus*). *Cereb Cortex* 29:3836–3863
- Atapour N, Worthy KH, Rosa MGP (2021) Neurochemical changes in the primate lateral geniculate nucleus following lesions of striate cortex in infancy and adulthood: implications for residual vision and blindsight. *Brain Struct Funct*. <https://doi.org/10.1007/s00429-021-02257-0>
- Baldwin MKL, Balaram P, Kaas JH (2017) The evolution and functions of nuclei of the visual pulvinar in primates. *J Comp Neurol* 525:3207–3226
- Beck PD, Kaas JH (1998) Thalamic connections of the dorsomedial visual area in primates. *J Comp Neurol* 396(3):381–398
- Benevento L, Rezak M (1976) The cortical projections of the inferior pulvinar and adjacent lateral pulvinar in the rhesus monkey (*Macaca mulatta*): an autoradiographic study. *Brain Res* 108:1–24
- Berman RA, Wurtz RH (2010) Functional identification of a pulvinar path from superior colliculus to cortical area MT. *J Neurosci* 30:6342–6354
- Berman RA, Wurtz RH (2011) Signals conveyed in the pulvinar pathway from superior colliculus to cortical area MT. *J Neurosci* 31:373–384
- Bourne JA, Morrone MC (2017) Plasticity of visual pathways and function in the developing brain: is the pulvinar a crucial player? *Front Syst Neurosci* 11:3
- Bourne JA, Rosa MGP (2006) Hierarchical development of the primate visual cortex, as revealed by neurofilament immunoreactivity: early maturation of the middle temporal area (MT). *Cereb Cortex* 16:405–414
- Bourne JA, Warner CE, Rosa MGP (2005) Topographic and laminar maturation of striate cortex in early postnatal marmoset monkeys, as revealed by neurofilament immunohistochemistry. *Cereb Cortex* 15:740–748
- Bridge H, Leopold DA, Bourne JA (2016) Adaptive pulvinar circuitry supports visual cognition. *Trends Cogn Sci* 20:146–157

- Bridge H, Bell AH, Ainsworth M, Sallet J, Premereur E, Ahmed B, Mitchell AS, Schüffelgen U, Buckley M, Tandler BC, Miller KL (2019) Preserved extrastriate visual network in a monkey with substantial, naturally occurring damage to primary visual cortex. *Elife* 8:e42325
- Bullier J, Kennedy H (1983) Projection of the lateral geniculate nucleus onto cortical area V2 in the macaque monkey. *Exp Brain Res* 53:168–172
- Burman KJ, Bakola S, Richardson KE, Yu HH, Reser DH, Rosa MGP (2015) Cortical and thalamic projections to cytoarchitectural areas 6Va and 8C of the marmoset monkey: connectionally distinct subdivisions of the lateral premotor cortex. *J Comp Neurol* 523:1222–1247
- Byne W, Fernandes J, Haroutunian V, Huacon D, Kidkardnee S, Kim J, Tatusov A, Thakur U, Yiannoulos G (2007) Reduction of right medial pulvinar volume and neuron number in schizophrenia. *Schizophr Res* 90:71–75
- Chalfin BP, Cheung DT, Muniz JA, de Lima Silveira LC, Finlay BL (2007) Scaling of neuron number and volume of the pulvinar complex in New World primates: comparisons with humans, other primates, and mammals. *J Comp Neurol* 504:265–274
- Chaplin TA, Yu HH, Rosa MGP (2013) Representation of the visual field in the primary visual area of the marmoset monkey: magnification factors, point-image size, and proportionality to retinal ganglion cell density. *J Comp Neurol* 521:1001–1019
- Chen D, Huang Y, Shi Z, Li J, Zhang Y, Wang K, Smith AD, Gong Y, Gao Y (2020) Demyelinating processes in aging and stroke in the central nervous system and the prospect of treatment strategy. *CNS Neurosci Ther* 26:1219–1229
- Cowey A, Alexander I, Stoerig P (2011) Transneuronal retrograde degeneration of retinal ganglion cells and optic tract in hemianopic monkeys and humans. *Brain* 134:2149–2157
- Cusick CG, Gould HJ III (1990) Connections between area 3b of the somatosensory cortex and subdivisions of the ventroposterior nuclear complex and the anterior pulvinar nucleus in squirrel monkeys. *J Comp Neurol* 292:83–102
- Cusick CG, Scriptor JL, Darenbourg JG, Weber JT (1993) Chemoarchitectonic subdivisions of the visual pulvinar in monkeys and their connectional relations with the middle temporal and rostral dorsolateral visual areas, MT and DLr. *J Comp Neurol* 336:1–30
- Dick A, Kaske A, Creutzfeldt OD (1991) Topographical and topological organization of the thalamocortical projection to the striate and prestriate cortex in the marmoset (*Callithrix jacchus*). *Exp Brain Res* 84:233–253
- Dineen JT, Hendrickson AE (1981) Age correlated differences in the amount of retinal degeneration after striate cortex lesions in monkeys. *Invest Ophthalmol vis Sci* 21:749–752
- Fox DM, Goodale MA, Bourne JA (2020) The age-dependent neural substrates of blindsight. *Trends Neurosci* 43:242–252
- Gallyas F (1979) Silver staining of myelin by means of physical development. *Neurol Res* 1:203–209
- Gao X, Deng P, Xu ZC, Chen J (2011) Moderate traumatic brain injury causes acute dendritic and synaptic degeneration in the hippocampal dentate gyrus. *PLoS One* 6(9):e24566
- Grieve KL, Acuña C, Cudeiro J (2000) The primate pulvinar nuclei: vision and action. *Trends Neurosci* 23:35–39
- Gundersen HJ, Jensen EB (1987) The efficiency of systematic sampling in stereology and its prediction. *J Microsc* 147:229–263
- Gutierrez C, Cola MG, Seltzer B, Cusick C (2000) Neurochemical and connectional organization of the dorsal pulvinar complex in monkeys. *J Comp Neurol* 419:61–86
- Hagan MA, Rosa MGP, Lui LL (2017) Neural plasticity following lesions of the primate occipital lobe: the marmoset as an animal model for studies of blindsight. *Dev Neurobiol* 77:314–327
- Hagan MA, Chaplin TA, Huxlin KR, Rosa MGP, Lui LL (2019) Altered sensitivity to motion of area MT neurons following long-term V1 lesions. *Cereb Cortex* 30:451–464
- Harting JK, Huerta MF, Frankfurter AJ, Strominger NL, Royce GJ (1980) Ascending pathways from the monkey superior colliculus: an autoradiographic analysis. *J Comp Neurol* 192:853–882
- Hendrickson A, Warner CE, Possin D, Huang J, Kwan WC, Bourne JA (2015) Retrograde transneuronal degeneration in the retina and lateral geniculate nucleus of the V1-lesioned marmoset monkey. *Brain Struct Funct* 220:351–360
- Hill CS, Coleman MP, Menon DK (2016) Traumatic axonal injury: mechanisms and translational opportunities. *Trends Neurosci* 39:311–324
- Homman-Ludiye J, Mundingano IC, Kwan WC, Bourne JA (2020) Extensive connectivity between the medial pulvinar and the cortex revealed in the marmoset monkey. *Cereb Cortex* 30:1797–1812
- Huo BX, Zeater N, Lin MK, Takahashi YS, Hanada M, Nagashima J, Lee BC, Hata J, Zaheer A, Grünert U, Miller MI, Rosa MGP, Okano H, Martin PR, Mitra PP (2019) Relation of koniocellular layers of dorsal lateral geniculate to inferior pulvinar nuclei in common marmosets. *Eur J Neurosci* 50:4004–4017
- Jones EG (2001) The thalamic matrix and thalamocortical synchrony. *Trends Neurosci* 24(10):595–601
- Jones EG (2007) *The thalamus*, 2nd edn. Cambridge University Press, Cambridge
- Kaas JH, Baldwin MKL (2020) The evolution of the pulvinar complex in primates and its role in the dorsal and ventral streams of cortical processing. *Vision (basel)* 4:3
- Kaas JH, Lyon DC (2007) Pulvinar contributions to the dorsal and ventral streams of visual processing in primates. *Brain Res Rev* 55:285–296
- Kaske A, Dick A, Creutzfeldt OD (1991) The local domain for divergence of subcortical afferents to the striate and extrastriate visual cortex in the common marmoset (*Callithrix jacchus*): a multiple labelling study. *Exp Brain Res* 84:254–265
- Kemether EM, Buchsbaum MS, Byne W, Hazlett EA, Haznedar M, Brickman AM, Platholi J, Bloom R (2003) Magnetic resonance imaging of mediadorsal, pulvinar, and centromedian nuclei of the thalamus in patients with Schizophrenia. *Arch Gen Psychiatry* 60:983–991
- Kennedy H, Bullier J (1985) A double-labeling investigation of the afferent connectivity to cortical areas V1 and V2 of the macaque monkey. *J Neurosci* 5:2815–2830
- Krishnamurthy LC, Champion GN, McGregor KM, Krishnamurthy V, Turabi A, Roberts SR, Nocera JR, Borich MR, Rodriguez AD, Belagaje SR, Harrington RM, Harris-Love ML, Harnish SM, Drucker JH, Benjamin M, Meadows ML, Seeds L, Zlatar ZZ, Sudhyadhom A, Butler AJ, Garcia A, Patten C, Trinastic J, Kautz SA, Gregory C, Crosson BA (2020) The effect of time since stroke, gender, age, and lesion size on thalamus volume in chronic stroke: a pilot study. *Sci Rep* 10:20488
- Lysakowski A, Standage GP, Benevento LA (1988) An investigation of collateral projections of the dorsal lateral geniculate nucleus and other subcortical structures to cortical areas V1 and V4 in the macaque monkey: a double label retrograde tracer study. *Exp Brain Res* 69:651–661
- Magon S, May A, Stankewitz A, Goadsby PJ, Tso AR, Ashina M, Amin FM, Seifert CL, Chakravarty MM, Müller J, Sprenger T (2015) Morphological abnormalities of thalamic subnuclei in migraine: a multicenter MRI study at 3 Tesla. *J Neurosci* 35:13800–13806
- Mahajan KR, Nakamura K, Cohen JA, Trapp BD, Ontaneda D (2020) Intrinsic and extrinsic mechanisms of thalamic pathology in multiple sclerosis. *Ann Neurol* 88:81–92

- Majka P, Bednarek S, Chan JM, Jermakow N, Liu C, Saworska G, Worthy KH, Silva AC, Wójcik DK, Rosa MGP (2021) Histology-based average template of the marmoset cortex with probabilistic localization of cytoarchitectural areas. *Neuroimage* 226:117625
- Marion CM, McDaniel DP, Armstrong RC (2019) Sarm1 deletion reduces axon damage, demyelination, and white matter atrophy after experimental traumatic brain injury. *Exp Neurol* 321:113040
- Meier PG, Maeder P, Kardon RH, Borruat FX (2015) Homonymous ganglion cell layer thinning after isolated occipital lesion: macular OCT demonstrates transsynaptic retrograde retinal degeneration. *J Neuroophthalmol* 35:112–116
- Melnick MD, Tadin D, Huxlin KR (2016) Relearning to see in cortical blindness. *Neuroscientist* 22:199–212
- Minagar A, Barnett MH, Benedict RH, Pelletier D, Pirko I, Sahraian MA, Frohman E, Zivadinov R (2013) The thalamus and multiple sclerosis: modern views on pathologic, imaging, and clinical aspects. *Neurology* 80:210–219
- Missler M, Eins S, Merker HJ, Rothe H, Wolff JR (1993a) Pre- and postnatal development of the primary visual cortex of the common marmoset. I. A changing space for synaptogenesis. *J Comp Neurol* 333:41–52
- Missler M, Wolff A, Merker HJ, Wolff JR (1993b) Pre- and postnatal development of the primary visual cortex of the common marmoset. II. Formation, remodelling, and elimination of synapses as overlapping processes. *J Comp Neurol* 333:53–67
- Mundinano IC, Kwan WC, Bourne JA (2019) Retinotopic specializations of cortical and thalamic inputs to area MT. *Proc Natl Acad Sci USA* 116:23326–23331
- Ogren M, Hendrickson A (1976) Pathways between striate cortex and subcortical regions in *Macaca mulatta* and *Saimiri sciureus*: evidence for a reciprocal pulvinar connection. *Exp Neurol* 53(3):780–800
- Pareto D, Garcia-Vidal A, Alberich M, Auger C, Montalban X, Tintoré M, Sastre-Garriga J, Rovira À (2020) Ratio of T1-weighted to T2-weighted signal intensity as a measure of tissue integrity: comparison with magnetization transfer ratio in patients with multiple sclerosis. *Am J Neuroradiol* 41:461–463
- Paxinos G, Watson C, Petrides M, Rosa MGP, Tokuno H (2012) The marmoset brain in stereotaxic coordinates. Academic, Amsterdam, London
- Perslson E, Maday S, Fu MM, Moughamian AJ, Holzbaur EL (2010) Retrograde axonal transport: pathways to cell death? *Trends Neurosci* 33:335–344
- Pollock A, Hazelton C, Henderson CA, Angilley J, Dhillon B, Langhorne P, Livingstone K, Munro FA, Orr H, Rowe FJ (2011) Interventions for visual field defects in patients with stroke. *Cochrane Database Syst Rev* 10:CD008388
- Pons TP, Kaas JH (1985) Connections of area 2 of somatosensory cortex with the anterior pulvinar and subdivisions of the ventroposterior complex in macaque monkeys. *J Comp Neurol* 240:16–36
- Purushothaman G, Marion R, Li K, Casagrande VA (2012) Gating and control of primary visual cortex by pulvinar. *Nat Neurosci* 15:905–912
- Ratliff WA, Mervis RF, Citron BA, Schwartz B, Rubovitch V, Schreiber S, Pick CG (2020) Effect of mild blast-induced TBI on dendritic architecture of the cortex and hippocampus in the mouse. *Sci Rep* 10:2206
- Rodman HR, Gross CG, Albright TD (1990) Afferent basis of visual response properties in area MT of the macaque. II. Effects of superior colliculus removal. *J Neurosci* 10:1154–1164
- Rosa MGP, Tweedale R, Elston GN (2000) Visual responses of neurons in the middle temporal area of new world monkeys after lesions of striate cortex. *J Neurosci* 20:5552–5563
- Royet JP (1991) Stereology: a method for analysing images. *Prog Neurobiol* 37:433–474
- Selemon LD, Begovic A, Rakic P (2009) Selective reduction of neuron number and volume of the mediodorsal nucleus of the thalamus in macaques following irradiation at early gestational ages. *J Comp Neurol* 515:454–464
- Shin KJ, Lee H-J, Park KM (2019) Alterations of individual thalamic nuclei volumes in patients with migraine. *J Headache Pain* 20:112
- Shipp S (2001) Corticopulvinar connections of areas V5, V4, and V3 in the macaque monkey: a dual model of retinal and cortical topographies. *J Comp Neurol* 439:469–490
- Soares JG, Gattass R, Souza AP, Rosa MGP, Fiorani M Jr, Brandão BL (2001) Connectional and neurochemical subdivisions of the pulvinar in Cebus monkeys. *Vis Neurosci* 18:25–41
- Stepniewska I, Kaas JH (1997) Architectonic subdivisions of the inferior pulvinar in New World and Old-World monkeys. *Vis Neurosci* 14:1043–1060
- Stepniewska I, Qi HX, Kaas JH (2000) Projections of the superior colliculus to subdivisions of the inferior pulvinar in New World and Old-World monkeys. *Vis Neurosci* 17:529–549
- Takakuwa N, Isa K, Onoe H, Takahashi J, Isa T (2021) Contribution of the pulvinar and lateral geniculate nucleus to the control of visually guided saccades in blindsight monkeys. *J Neurosci* 41:1755–1768
- Trojanowski JQ, Jacobson S (1997) The morphology and laminar distribution of cortico-pulvinar neurons in the rhesus monkey. *Exp Brain Res* 28:51–62
- Ungerleider LG, Galkin TW, Mishkin M (1983) Visuotopic organization of projections from striate cortex to inferior and lateral pulvinar in rhesus monkey. *J Comp Neurol* 217:137–157
- Ungerleider LG, Desimone R, Galkin TW, Mishkin M (1984) Subcortical projections of area MT in the macaque. *J Comp Neurol* 223:368–386
- Walker AE (1938) The primate thalamus. University of Chicago Press, Chicago
- Warner CE, Goldshmit Y, Bourne JA (2010) Retinal afferents synapse with relay cells targeting the middle temporal area in the pulvinar and lateral geniculate nuclei. *Front Neuroanat* 4:8
- Warner CE, Kwan WC, Wright D, Johnston LA, Egan GF, Bourne JA (2015) Preservation of vision by the pulvinar following early-life primary visual cortex lesions. *Curr Biol* 25:424–434
- Williams RW, Rakic P (1988) Three-dimensional counting: an accurate and direct method to estimate numbers of cells in sectioned material. *J Comp Neurol* 278:344–352
- Wolf HK, Buslei R, Schmidt-Kastner R, Schmidt-Kastner PK, Pietsch T, Wiestler OD, Blumcke I (1996) NeuN: a useful neuronal marker for diagnostic histopathology. *J Histochem Cytochem* 44:1167–1171
- Yu HH, Chaplin TA, Egan GW, Reser DH, Worthy KH, Rosa MGP (2013) Visually evoked responses in extrastriate area MT after lesions of striate cortex in early life. *J Neurosci* 33:12479–12489
- Yu HH, Atapour N, Chaplin TA, Worthy KH, Rosa MGP (2018) Robust visual responses and normal retinotopy in primate lateral geniculate nucleus following long-term lesions of striate cortex. *J Neurosci* 38:3955–3970

Publisher's Note Springer Nature remains neutral with regard to jurisdictional claims in published maps and institutional affiliations.